BOREAS An international journal of Quaternary research

High-resolution stratigraphy of Scandinavian coastal archaeological settlements: the case of Håkonshella, W Norway

ARNALD PUY, ANDREA L. BALBO, CAMILLA ZINSLI AND MORTEN RAMSTAD

BOREAS

Puy, A., Balbo, A. L., Zinsli, C. & Ramstad, M. 2016 (July): High-resolution stratigraphy of Scandinavian coastal archaeological settlements: the case of Håkonshella, W Norway. *Boreas*, Vol. 45, pp. 508–520. 10.1111/bor.12166. ISSN 0300-9483.

The stratigraphy of Scandinavian open-air archaeological settlements is usually characterized as homogeneous, highly enriched in decomposing organic matter and poor in biogenic carbonates such as shells or bones. As a result, stratigraphies are often difficult to read in the field and settlement sequences may pass unnoticed by archaeologists. Here we show how the integration of bulk analyses, soil micromorphology, X-ray fluorescence (XRF) core scanning and multivariate statistics can help in overcoming such limitations. We use the case study of Håkonshella 8, a Mesolithic hunter-fisher-gatherer settlement located in Bergen (W Norway). Fluctuations in the organic matter content, geochemical proxies (mainly P, Ga, Ti and the Si/Al ratio) and redoximorphic features highlight four cycles of site occupation and abandonment in an otherwise massive anthropogenic deposit. Following these settlement sequences, the site was covered by colluvium from nearby slopes over which a waterlogged soil formed. The approach used in Håkonshella has the potential to improve our capacity to interpret organically enriched anthropic deposits formed in coastal Scandinavia and in similar climatic regions.

Arnald Puy (arnald.puy@gmail.com), Institute of Geography, University of Cologne, Albertus-Magnus-Platz, Cologne 50923, Germany; Andrea L. Balbo, Complexity and Socio-Ecological Dynamics (CaSEs), Department of Archaeology and Anthropology, Institució Milà i Fontanals (IMF), Consejo Superior de Investigaciones Científicas (CSIC), ClEgipcíaques 15, Barcelona 08001, Spain; Camilla Zinsli and Morten Ramstad, Section for Cultural Heritage Management, University Museum of Bergen, J. Frielegt. 1, 5020 Bergen, Norway; *received 20th July 2015, accepted 14th December 2015.*

The need for pin-sharp screening tools to understand stratigraphical sequences is compelling in Scandinavian open-air coastal archaeological sites. In these contexts the sequences are usually shallow, massive black and highly enriched in decomposed organic matter, with almost no biogenic carbonate remains such as shells or bones. Postdepositional processes and diagenesis caused by soil acidity and leaching significantly alter the archaeological record and pose significant challenges in terms of excavation methodology, stratigraphical control and phasing of cultural deposits (Simpson 1999; Estévez *et al.* 2013). In these problematic situations, with some exceptions (Balbo *et al.* 2010a; Briz Godino *et al.* 2011; Villagrán *et al.* 2011), excavation often proceeds by artificial cuts of homogeneous deposits. Archaeological sequences are defined in post-excavation phases largely based on the combination of accelerated mass spectrometry (AMS) dating with the qualitative and quantitative study of archaeological materials (Olsen 1992; Bergsvik 2002; Ramstad 2005; Bjerck *et al.* 2008).

X-ray spectrometers have been widely used in archaeometry to characterize archaeological materials such as minerals, rocks, sediments, pottery shards, bones, paintings, glasses, coins and tokens, amongst others (Piga *et al.* 2009; Duran *et al.* 2011; Shilstein & Shalev 2011; Forouzan *et al.* 2012; Liu *et al.* 2012; Attaelmanan & Mouton 2014; Columbu *et al.* 2014; Hunt & Speakman 2015). With some exceptions (Finlayson *et al.* 2006; Iriarte *et al.* 2013; Kalbe *et al.* 2014), XRF core scanning –closely spaced, high-resolution multi-elemental analysis of split sediment or rock slabs – has been much less applied in archaeological research. Mostly developed for the study of palaeoenvironmental records, XRF core scanning has become essential as a relatively fast, nondestructive method to precisely assess the geochemistry of sediment sequences extracted from wetlands (Poto *et al.* 2013; Martin *et al.* 2014; Schittek *et al.* 2014), the sea floor (Frigola *et al.* 2007; Moreno *et al.* 2012) or the bottom of lakes (Unkel *et al.* 2008; Morellón *et al.* 2009; Calò *et al.* 2013), allowing detailed information on long-term climatic shifts and landscape evolution to be obtained. Due to its millimetric resolution, the application of XRF core scanning in archaeological contexts has great potential for identifying microstratigraphical layers related to settlement sequences virtually undetectable in the field.

Here we show the potential of combining established geoarchaeological techniques, such as soil micromorphology and bulk sediment analyses, with XRF core scanning and multivariate statistics to assess and differentiate the microstratigraphy of Scandinavian anthropic deposits. We use the case study of Håkonshella 8, an open-air, hunter-fisher-gatherer coastal Mesolithic settlement located to the W of Bergen, W Norway. The main aims of our study were (i) to refine our understanding of the site occupation phases, and (ii) to identify depositional and postdepositional processes that have contributed to the formation of the site.

DOI 10.1111/bor.12166 © 2016 Collegium Boreas. Published by John Wiley & Sons Ltd

Study area

Håkonshella 8 (UTM 32 289287 E–6696005 N) is located about 10 km W of Bergen, W Norway (Fig. 1A), at a small peninsula facing the strong tidal current Vatlestraumen towards the W. It is located near the cross-point of three fjord systems, Hjeltefjorden to the NW and N, Byfjorden to the NE and Grimstad-

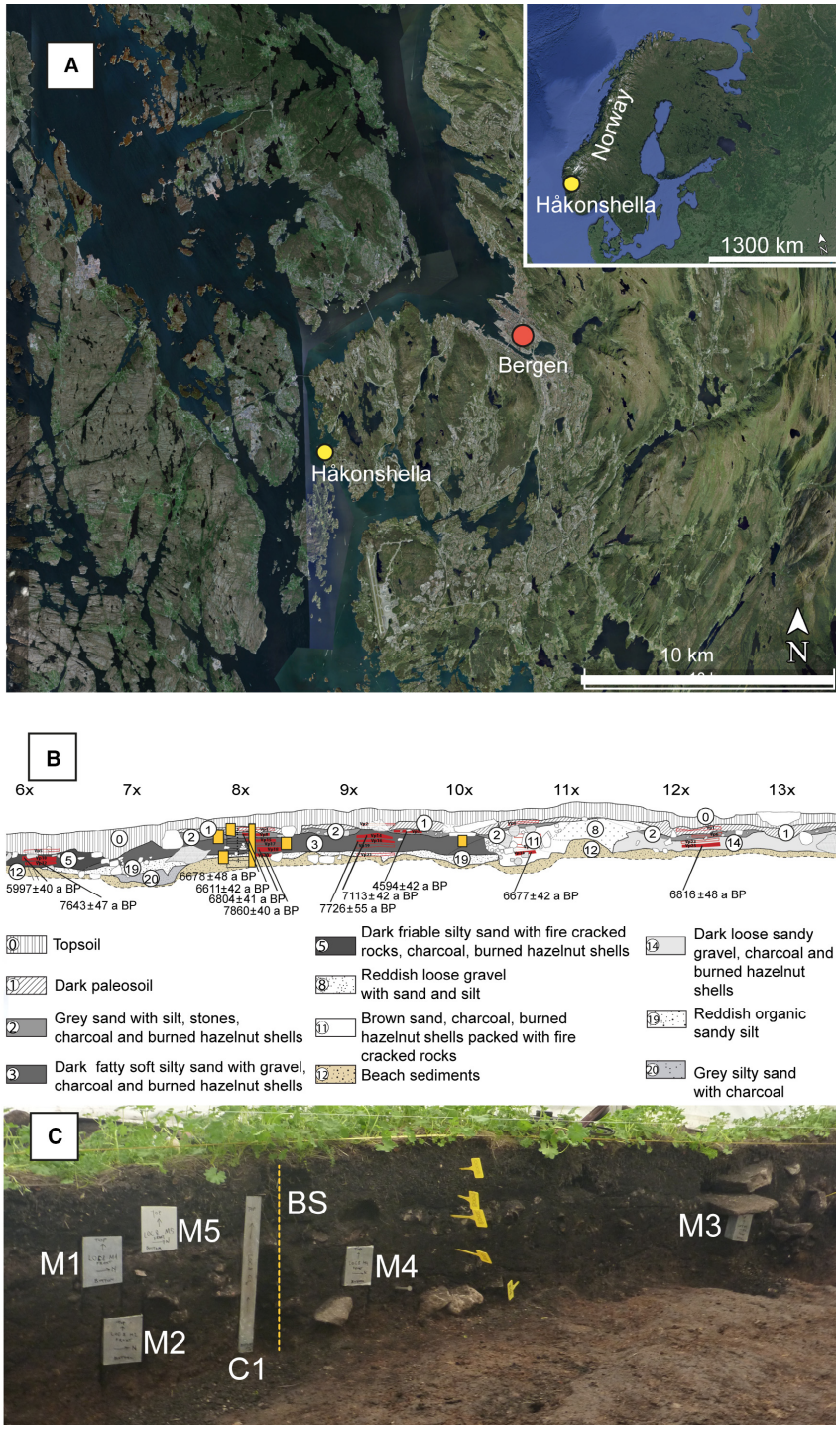

Fig. 1. The Mesolithic site of Håkonshella 8. A. Location of Håkonshella (maps from Google Earth Pro 2015). B. Stratigraphy of the sampled profile. The numbers in circles label the layers identified during fieldwork. The dark layer (number 3) is the Mesolithic deposit. C. Photograph of the stratigraphical profile and location of the samples: C1 (XRF core scanning), M1–M5 (soil micromorphology) and BS (bulk samples). This figure is available in colour at http://www.boreas.dk.

fjorden to the SE. The local climate is temperate oceanic, with a mean annual temperature in 2014–2015 of 7.5 °C (highest 31.4 °C and lowest −6.3 °C) and a mean annual precipitation of 2250 mm (climatic data retrieved from Bergen, Meteorologisk Institut). Geologically, the region falls within the Minor Bergen Arc, formed by three highly strained rock units: the Nordåsvatn Complex (with metagabbro, amphibolite, greenstone and greenschist), the Storetveit group (a metasedimentary cover consisting of green polymict conglomerate) and the Gamlehaugen Complex (formed by entangled psammitic metasediments and mylonitic gneisses) (Fossen 1989). The most common soils are podzols, characterized by a typically ash-grey upper subsurface horizon bleached by loss of organic matter and iron oxides, leading often to the formation of an albic horizon (FAO 2006). Conifers and broad-leaved trees abound, as well as holly and bell heather.

There has been extensive research on the Mesolithic of coastal Norway over the past 30 years (Bjerck 2008). The highest concentrations of Mesolithic settlements have been identified along the W Norwegian coast, where the presence of islands, inlets, skerries, bays and headlands provided more sheltered seascapes and richer marine biotopes than those found in continental Europe (Bjerck 2005). Most of the sites were shore-bound and coastal settlement areas were typically in use over periods of several thousands of years (Ramstad 2005). Such long settlement histories and the preservation of coastal sites were favoured in some portions of W Norway by the postglacial isostatic uplift of Scandinavia, which limited coastal submersion following Holocene deglaciation and the consequent sea-level rise (Bondevik & Svendsen 1998; Bailey & Flemming 2008; Balbo *et al.* 2010b). As a result of long settlement histories and local climatic conditions, anthropic layers within coastal Mesolithic sites appear as fat, dark, charcoal-rich massive deposits mixed with fire-cracked rocks and heavily decomposed bone material (Bjerck 2008).

Excavated between 2011 and 2012, Håkonshella 8 contained one of the earliest dated Mesolithic dwellings in W Norway (Bjerck 2008; Åstveit 2009). Håkonshella 8 is now located 14 m a.s.l. due to isostatic uplift, but was shore-bound at the time of Mesolithic occupation. After mechanical stripping of the turf grown on top of the archaeological area, archaeological layers were excavated over 66 m^2, removing a total of 12.58 m^3 of sediment. The removed sediments were water-sieved in 2–4 mm meshes. Neither organic material nor biogenic calcium carbonate remains were recovered during the excavation. The total number of finds was 12 249, consisting of tools and waste material from lithic production.

Material and methods

Sampling and physico-chemical analyses

The sampling was concentrated on a portion of the stratigraphical profile 47 cm thick and consisting of five superposed layers (0, 1, 2, 3, 12), including a Mesolithic floor. Layer 0 (0–12 cm below ground level; b.g.l.) was the current topsoil, black and highly enriched in organic matter. It was dotted with white fine material and abundant roots from the grass growing on top at the time of excavation. Layer 1 (12–17 cm b.g.l.) was characterized in the field as a black palaeosoil, with little mineral component, clayish and fatty in texture. Layer 2 (17–22 cm b.g.l.) was dark grey and consisted of sand, abundant angular clasts and subrounded boulders. Layer 3 (22–37 cm b.g.l.) was interpreted as corresponding to the Mesolithic occupation, showing some mineral inclusions from layer 2 and strong bioturbation in the form of worm and root channels. It mostly consisted of homogeneous, massive reddish-brown sand mixed with charred material and highly decomposed organic matter. Finally, layer 12 (37–45 cm b.g.l.) was very dusky red and mainly composed of sandy and silty quartz grains. It was very bioturbated and partially mixed with layer 3, including also small weathered angular clasts (Fig. 1B).

Three sets of samples were taken from the exposed stratigraphy at Håkonshella 8, on which physico-chemical analyses were performed in the laboratory (Fig. 1B, C).

Bulk samples (BS) for loss on ignition (LOI) were collected bottom-up from the stratigraphical profile every 2 cm and burned for 4 h at 105, 400, 480 and 950 °C to estimate the proportion of water, organic matter, coal and calcium carbonate, respectively (Heiri *et al.* 2001).

Five undisturbed blocks for soil micromorphology (M1–M5), including intact strata and the transition between strata, were also taken from the stratigraphical profile using Kubiena boxes (10×8×8 cm). Thin sections were prepared at SCT Micromorfologia de Sòls i Anàlisis d'Imatges Laboratory, Universitat de Lleida, Spain. After drying for 2 months at room temperature, the collected undisturbed blocks were impregnated with a mixture of Palatal polyester with styrene (100–200 mL L^{-1}), MEK (5–7 mL L^{-1}) and two drops of cobalt octoate. Following impregnation, samples were left to dry for another 6 weeks. Thin sections were cut with a diamond blade and polished with a machine Brot Tech® 1.03.12.P until a thickness of 20 μm was achieved. Analysis of thin sections was carried out with Leica® MZ9.5 and DM2500 microscopes, as well as with a Keyence® VHX-2000. The micromorphological description and interpretation

were based on Courty *et al.* (1989), Stoops (2003) and Stoops *et al.* (2010).

A continuous and undisturbed sediment sample across the stratigraphical profile (8–45 cm b.g.l.) was collected using an aluminium box (C1, 37×4×4 cm), which was encased in plastic film and aluminium wrap and stored in cold conditions before analysis. C1 was scanned at a resolution of 5 mm using an AVAATECH X-ray fluorescence core scanner equipped with a Rh tube at the XRF Core Scanner Laboratory of the Marine Geosciences GCR, Departament d'Estratigrafia, Paleontologia i Geociències Marines, Universitat de Barcelona. The core was covered with a 4 μm thin SPEXCerti Pret Ultralene 1 foil to avoid contamination and desiccation of the sediment during the measurements. The XRF core scanner was set at 10- and 25-s measurement times, 10 and 30 kV X-ray voltages, and 1.4 and 2.0 mA X-ray currents for major and trace elements, respectively. Layer 0 (8–12 cm) and the bottom of layer 12 (42–45 cm) were not scanned due to the poor preservation of the material in the core. Raw elemental data obtained after XRF core scanning were processed using the WIN AXIL (Analysis of X-ray Spectra by Iterative Least square) package from Canberra Eurisys to collect intensity data in counts per second (cps). In order to correct for changes in porosity and lithology along the core, we normalized the cps for each element by the total counts at each depth interval of all elements except Ag and Rh, which tend to be biased by the signal generation (Cuven *et al.* 2011; Bahr *et al.* 2014). We also used log-ratios to account for a robust representation of elemental ratios (Weltje & Tjallingii 2008; Grützner & Higgins 2010), selected to precise enrichments and depletions of mobile elements and diagenetic processes against detrital input. Al was chosen as a normalization element due to its acceptable counts along the core (mean of 161.0, 1254.08 at a 95% confidence interval) and its proven suitability in sedimentary sequences with strong fluctuations in the organic matter content (Löwemark *et al.* 2011), as for Håkonshella (Figs 2, 3). The final data set retained for analysis included eight elements (Al, Si, P, K, Ti, Ga, Rb and Zr) and five elemental ratios (Fe/Al, Mn/Fe, Si/Al, K/Al and Zr/Rb) and can be found in Table S1 and Figs 2, 3.

Data analyses

Factor analysis (FA) was carried out on the eight retained elements using XLStat Pro® version 2015.2. The aim was to explain the covariance between elements, identify underlying latent variables and reduce them to their common factor patterns. The Bartlett's test (p<0.05), the Kaiser–Meyer–Olkin measure of sampling adequacy (KMO, 0.71) and the Cronbach's alpha (0.82) indicated that the data set was factorizable and showed a high internal consistency (Cronbach 1951; Kaiser 1974). We thus ran the FA with a principal component extraction method after standardizing the data set to zero mean and unit variance. As communalities for each variable were >0.73, we assumed that more than three quarters of each variable's variance was accounted for by the factor solution. We

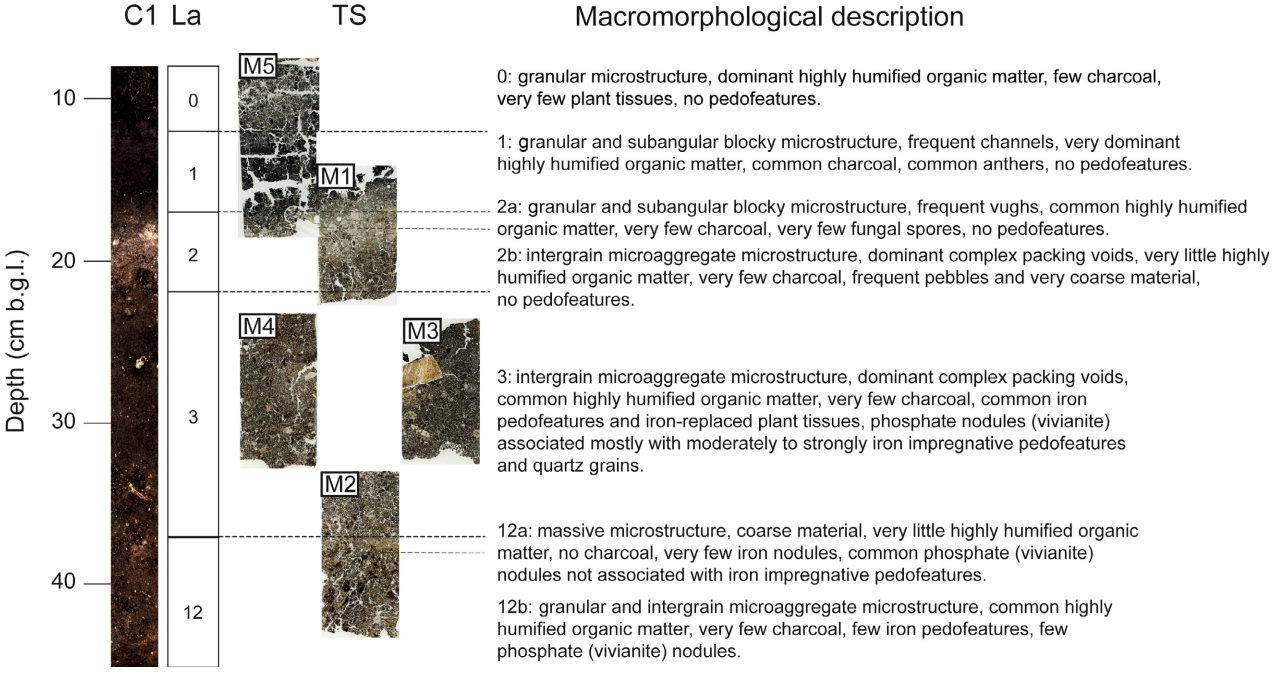

Fig. 2. Correspondence between the sediment core (C1), stratigraphy (La), thin sections (TS, M1–M5) and description of the thin sections. This figure is available in colour at http://www.boreas.dk.

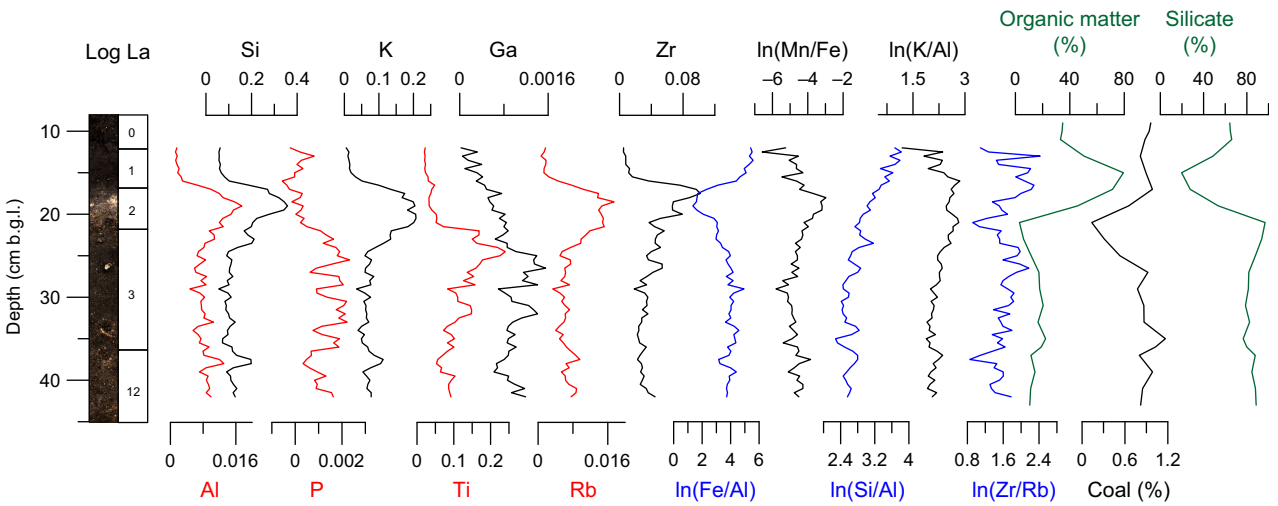

Fig. 3. Results of the physico-chemical analyses. Values for individual elements have been normalized by the total counts at each depth interval for all elements except Ag and Rh. Elemental ratios have been normalized as ln(ratios). This figure is available in colour at http://www.boreas.dk.

retained for analysis factors 1 and 2, as they had an eigenvalue higher than 1 and accounted for more than 80% of the cumulative variability, thus fulfilling two important conditions for a factor analysis (Kaiser 1960; Jolliffe 2002). A Varimax rotation with Kaiser normalization was applied to minimize the number of variables with a high loading on each component and ease the interpretation of variable–factor correlations (Kaiser & Rice 1974). The rotated solution had no outliers (scores higher or lower than ±3) and exhibited 'simple structure', indicating that each variable strongly loaded on just one single factor (Thurstone 1947).

Radiocarbon dating

The chronological characterization for the Mesolithic occupation of Håkonshella 8 was carried out using AMS. Dating was performed at Tandem Laboratory, University of Uppsala, Sweden, and at Beta Analytic on hazelnut remains extracted from the sediment sequence near transition boundaries between different sediment deposition phases. Dates were calibrated using OxCal v4.2 (Bronk Ramsey 2009) and the IntCal13 calibration curve (Reimer *et al.* 2013) (Table 1).

Results

Loss on ignition

The organic matter content of layer 1 (79–71%) was significantly ($p \leq 0.0001$) higher than those of layers 2 (3–5%) and 3 (11–22%). Layer 2 showed the highest content of silicate residue (96–93%), whereas $CaCO_3$ contents were negligible throughout the stratigraphical profile (<0.03%). As organic matter values along layer 3 seemed to roughly concur with peaks in P, Ga and the Si/Al ratio after visual inspection of the XRF data set (Fig. 3), we averaged the XRF data every 2 cm in layer 3 to correlate with the corresponding 2 cm from the LOI samples. The results indicated that organic matter correlated moderately and positively with the Si/Al ratio ($r = 0.56$, $p = 0.14$), strongly and negatively

Table 1. AMS dates.

Lab. code	Layer	Sample	Weight (g)	^{14}C a BP	Cal. 1 sigma BC	Cal. 2 sigma BC
Ua-44660	2	Hazelnut	0.29	4594±42	3498–3139	3516–3108
Ua-44659	2	Hazelnut	0.26	6678±48	5639–5558	5701–5511
Ua-44668	5	Hazelnut	0.21	5997±40	4942–4837	4993–4791
Ua-44667	5	Hazelnut	0.20	7643±47	6561–6440	6591–6431
Ua-44666	11	Hazelnut	0.20	6677±42	5636–5560	5666–5521
Ua-44665	3	Hazelnut	0.22	7113±42	6030–5924	6062–5903
Ua-44664	3	Hazelnut	0.16	6611±42	5615–5514	5620–5486
Ua-44663	3	Hazelnut	0.06	7726±55	6604–6492	6647–6463
Ua-44662	3	Hazelnut	0.21	6804±41	5725–5662	5746–5630
Beta-344208	19/12	Hazelnut	0.14	7860±40	6766–6642	6984–6597
Ua-44661	14	Hazelnut	0.52	6816±48	5735–5661	5790–5629

with Ga ($r = -0.81$, $p = 0.015$), and had a very weak negative correlation with P ($r = -0.16$, $p = 0.69$).

Soil micromorphology

The layers differ in their degree of coarse and fine material, pedality and abundance of phosphates and iron pedofeatures. Layer 0 represents the current soil surface and is characterized by a granular microstructure and a double-spaced equal/coarse enaulic c/f-related distribution, with the coarse material decreasing downwards (Fig. 4A). The mineral fraction is entirely lacking in layer 1, which fully consists of mammillated, unaccommodated, moderately to strongly developed subangular blocky peds up to 2000 μm in diameter formed by highly decomposed organic matter (Fig. 4B). Frequent anthers about 300–500 μm in diameter containing hundreds of pollen grains (20–30 μm wide) were also identified in layer 1 (Fig. 4C, D). The coarsest material was found in layer 2, formed by dominant subangular and subrounded polycrystalline quartz grains (up to 5 mm in diameter) with sutured crystals, dominant K-feldspar (orthoclase) and frequent pebbles, very few plagioclase feldspar and shales (Fig. 4E–H). Such minerals are also present in layers 1, 3 and 12, although in much smaller amounts. Signs of weathering are clearly visible in microfacies 2a, with some minerals showing parallel linear and cross-linear patterns of alteration. Layer 3 mainly differs from layers 1–2 by the higher frequency of iron and phosphate impregnative pedofeatures. Phosphate nodules, mostly vivianite (appearing as

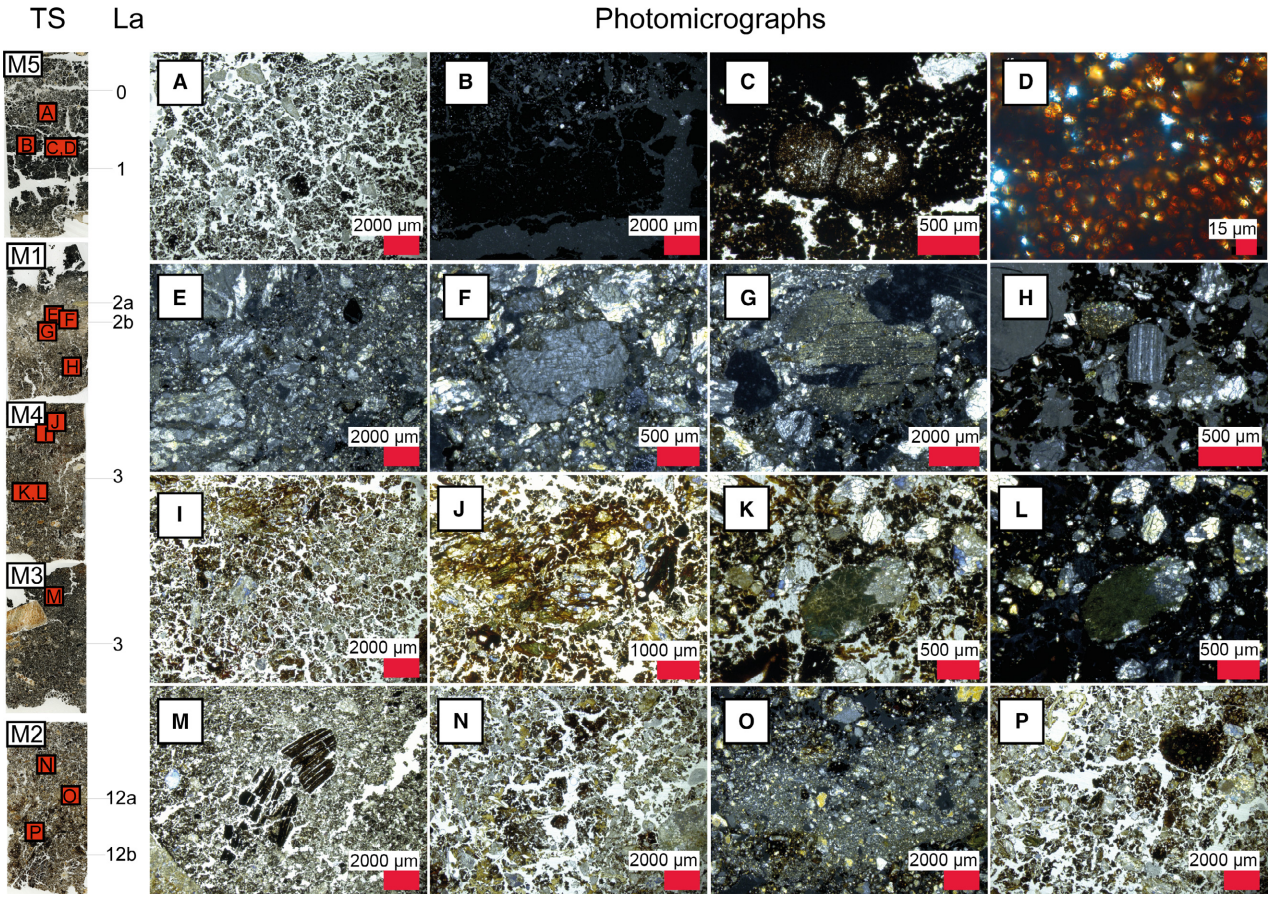

Fig. 4. Correspondence between thin sections (TS, M1–M5), layers (La) and location of the photomicrographs (red squares), taken under plane polarized light (PPL) and cross-polarized light (XPL). A. Groundmass from layer 1, showing a granular microstructure and a double-spaced equal enaulic c/f related distribution (PPL). B. Boundary between layer 0 (top) and 1 (bottom). Note the lack of coarse material and the well-developed subangular blocky peds in layer 1 (XPL). C. Anthers, probably of *Alnus* sp. (PPL). D. Detail of the pollen grains within the anther shown on C. (XPL). E. Groundmass of layer 2 (XPL). F. K-feldspar (orthoclase) in layer 2. Note the cracks along crystallographical planes (cleavage) (XPL). G. Shale in layer 2. Note the breaks along laminations, parallel to the bedding, and the presence of very fine sand grains embedded in the rock (XPL). H. Plagioclase feldspar with characteristic twinning in layer 2 (XPL). I. Groundmass of layer 3 with aggregates and coarse material moderately to strongly impregnated by iron (PPL). J. Phosphate nodules (green colour) associated with iron impregnative pedofeatures, pointing towards vivianite (PPL). K. Phosphate impregnation of a polycrystalline quartz grain (PPL). L. Same as K. (XPL). M. Fragmented charcoal in layer 3 (PPL). N. Groundmass of the lowermost part of layer 3, showing clay nodules and strongly impregnated clay pedofeatures (PPL). O. Detail of microfacies 12a, composed of coarse to medium sand grains with no fine material (XPL). P. Groundmass of layer 12, showing strongly impregnated iron pedofeatures, fine material and phosphate nodules. This figure is available in colour at http://www.boreas.dk.

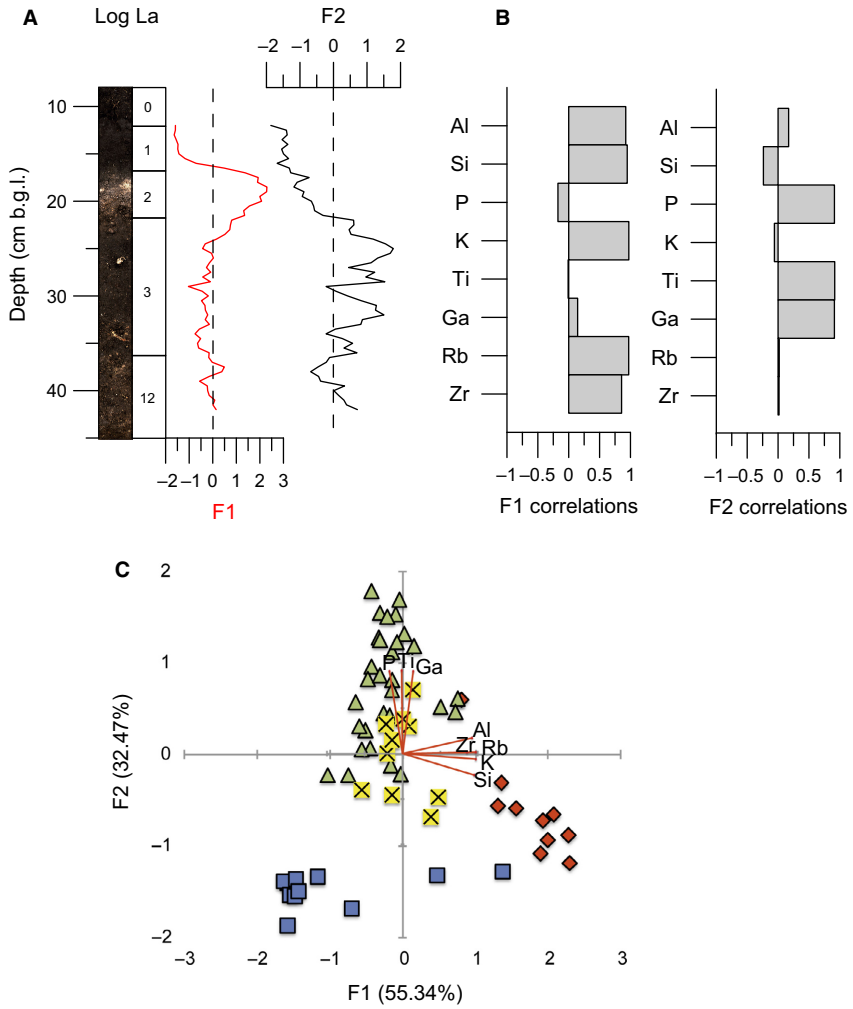

Fig. 5. Results of the factor analysis (Varimax-rotated with Kaiser normalization). A. Factors against composite depth. B. Correspondences between factors and variables. C. Biplot for F1 and F2. Blue squares = layer 1; red diamonds = layer 2; green triangles = layer 3; yellow crosses = layer 12. This figure is available in colour at http://www.boreas.dk.

radial aggregates with a greenish-blueish colour under plane-polarized light), were identified with moderately to strongly impregnated iron pedofeatures, quartz grains and highly decomposed organic matter (Fig. 4I–L). Iron coatings and hypocoatings were also identified in thin sections from layer 3, as well as fragments of plant remains and clay-replaced plant tissues (Fig. 4M, N). Layer 12 is separated from layer 3 by microfacies 12a, which has a massive structure, very dominant subangular and subrounded polycrystalline quartz grains up to 500 μm in diameter and very little organic matter. Phosphate nodules and iron impregnative pedofeatures, although lacking in microfacies 12a, appear again in layer 12 along with finer material and more organic matter (Fig. 4O, P).

Geochemistry

Figure 3 shows the results from the XRF core scanning. The down-core fluctuation of the analysed elements clearly corresponds with four out of the five layers identified in the field on the basis of their composition, colour and structure. The transition between layers 1–2 is characterized by an increase in Al, Si, K, Rb, Zr and Mn/Fe and by a decline in Fe/Al, Si/Al, K/Al and Zr/Rb. Layer 3 shows a marked increase in P, Ti, Ga and Fe/Al in relation to layer 2, as well as a slight increase in Zr/Rb and K/Al at the topmost part of the layer. It also appears depleted in Mn/Fe compared to layer 2. The transition between layers 3 and 12 does not clearly show any change in the pattern of any variable.

Figure 5A presents the variations of the factors (Fs) against composite depth, vertically displaying the contribution of each of the 61 observations to the new vectorial space defined by the FA (Morellón *et al.* 2009; Ferro-Vázquez *et al.* 2014), whereas Fig. 5B reports the correlations between the variables and each factor (F), respectively. We retained for analysis F1 (eigenvalue of 4.43) and F2 (eigenvalue of 2.58), which

accounted for 87.8% of the variability. High positive F1 scores characterize layer 2, whereas high positive F2 scores were attained throughout layer 3 and the topmost part of layer 12, with four clear peaks at 25, 28, 32 and 36 cm b.g.l. The relationship between the observations in the layers and the variables is also sharply visible in a biplot (Fig. 5C), with P, Ti and Ga clearly associated with layers 3 and 12 and Al, Zr, Rb, K and Si linked to layer 2.

Radiocarbon dating

The radiocarbon dates obtained from layer 3 indicated a Mesolithic occupation spanning 6647–6463 to 5620–5486 BC (2σ) (Table 1).

Discussion

The discussion will focus on layers 1–12, top to bottom. Layer 0 will not be considered as it represents the current soil surface and was not scanned through XRF.

Mineral and organic matter

F1, which explained 55.33% of the variability, is interpreted as 'mineral input' due to high positive contribution of variables related to siliciclastic deposits, such as Al, Si, K, Rb and Zr. Higher positive F1 scores thus reflect higher clast contents (layer 2), whereas higher negative scores indicate a lack of coarse material and predominance of organic matter (layers 1 and 3).

The elements that positively contribute to F1 are found in sandstones, feldspars and shales, which were widely identified in thin sections from layer 2 (Fig. 4E–H). K is found in orthoclase feldspars, whereas Zr and Rb tend to respectively be enriched in coarser (e.g. quartz, feldspar) and finer grains like clay materials (e.g. claystones, shales). The Zr/Rb ratio has thus been traditionally used as a granulometry proxy, with higher ratios pointing towards coarser-grained units and lower ratios reflecting finer-grained material (Dypvik & Harris 2001; Chen *et al.* 2006). Although it has been generally assumed that Zr/Rb ratios are not significantly altered by postdepositional weathering, some studies have found that Rb is much more mobile than Zr and that it can be lost from the profile when chemical alteration of K-feldspar minerals is high (Hodson 2002; Liu *et al.* 2006). Rb can also substitute for K in the crystal lattice of K-feldspars, which are commonly associated with coarse silt and sand fractions (Wedepohl 1971; Kylander *et al.* 2011), thus lowering the Zr/Rb ratios in coarse-sized layers. Under these circumstances the Zr/Rb ratio is unreliable as a proxy for granulometry.

K-feldspar diagenesis seems to have been an important process on the topmost horizon of layers 1, 2 and 3. This is suggested by low K/Al ratios, which have been used as a proxy for severe chemical diagenesis (Hu *et al.* 2013; Clift *et al.* 2014), with lower ratios suggesting higher weathering of K-feldspars (Fig. 3). Micromorphological signs of weathering such as parallel linear and cross-linear patterns of alteration in microfacies 2 also point towards K-feldspar dissolution (Fig. 4E). Moreover, the strong and significant ($r = 0.97$, $p < 0.0001$) correlation between K and Rb throughout C1, along with the lack of correlation of Ti with K ($r = -0.05$, $p = 0.68$), respectively indicate that K-feldspars might be a major source of Rb and that fine grains might not be relevant hosts for Rb (Kylander *et al.* 2011). This explains why the highest Zr/Rb ratios are not found in layer 2 but in layers 1 and 3, despite the former being coarser and comparatively enriched in the mineral fraction in thin sections. The lack of fine material and soil aggregates within layer 2, along with the absence of the main micromorphological features related with solifluction deposits (well-developed preferred clasts orientation perpendicular to contours and platy structure, see Mücher *et al.* 2010), indicate that layer 2 formed after an energetic event of erosion and deposition (Fig. 4E–H).

Mn/Fe ratios have been regarded as a proxy for redoximorphic conditions, with lower values usually indicating anoxic environments (Davison 1993; Koinig *et al.* 2003; Haenssler *et al.* 2014). Low Mn/Fe ratios are found in organic-rich layers such as 1 and 3, whereas higher ratios characterize layer 2. The latter is explained by the detrital nature of layer 2: with all other things being equal, the deposition and diagenesis of Mn-bearing rocks such as sandstones and shales lead to an increase in the Mn content of the sediment, therefore increasing the Mn/Fe ratio. In any case, organic matter tends to decrease the soil redox potential in wet soils both in absolute and relative terms, as humic substances are key in immobilizing Fe and Mn following reduction to soluble Fe^{2+} and Mn^{2+}, respectively (Graham *et al.* 2002; Gardiner & James 2012). This concurs with low Mn/Fe values in layers 1 and 3, indicating a lack of air and waterlogging. The peak in Fe/Al at the top of layer 1 probably resulted from the precipitation of Fe to $FeCO_3$, leading to a redox enrichment where the water table fluctuated (Schittek *et al.* 2014). Layer 1 was thus probably a seasonally waterlogged soil formed *in situ* with negligible contribution of sediments from the surrounding slopes, as indicated by negative F1 scores, scarcity of minerals within the groundmass and its moderate to strongly developed subangular blocky peds. Anthers present in layer 1 point towards *Alnus* sp. (W. Out, pers. comm. 2013), a genus comprising about 30 species of monoecious trees and shrubs common in palustrine, lacustrine and wet landscapes (Fig. 4C, D). Both the abundance and the size of the anthers suggest that they were local in origin.

Anthropic activity

F2, which explained 32.46% of the variability, is interpreted as 'anthropic activity' due to the high positive contributions of variables that can be linked to human influence, such as P, Ga and Ti. High positive F2 scores are found in layer 3, with four clear peaks at 25, 28, 32 and 36 cm b.g.l., probably representing at least four different occupation phases between 6647–6463 and 5620–5486 BC (2σ). The highest negative F2 scores are found in layers 1–2, indicating the end of the settlement. Scores close to zero are attained along layer 3 and were interpreted as temporary abandonments of the site (Fig. 5).

P has been widely used in archaeology as an anthropic proxy, as prolonged human occupations increase soil P as a result of burning of organic material, accumulation of human and animal waste, deposition of ash from hearths, decomposition of food remains, deposition of burials and/or fertilization (Bethell & Máté 1989; Holliday & Gartner 2007). When humans add P to the soil, it mostly accumulates at the site of deposition, and it is less susceptible to leaching, oxidation, reduction or plant uptake than other elements such as C, N, S or Mg (Holliday & Gartner 2007). As layer 3 showed 65.52 times more P cps than layer 1 and four to seven times less organic matter, we considered human activity to be the most plausible factor responsible for the enhancement of P in layer 3. In this context, vivianite, whose presence was confirmed in thin sections from layer 3, is a Fe-phosphate mineral that has been related to human waste in archaeological settings (Karkanas & Goldberg 2010). It is very stable under anoxic conditions (Miot *et al.* 2009) and indicates that layer 3 was poorly oxygenated and enriched in Fe (McGowan & Prangnell 2007).

The other elements that contributed positively to F2 are Ga and Ti. Ga is a relatively stable trace element that can be found in feldspar or micas, in soils associated with Fe and Mn hydroxides, in the atmosphere (although in very low concentrations) and in plant and human tissues (Kabata-Pendias & Mukherjee 2007). Significant amounts of Ga can also enter the soil as fly ash during or after combustion activities (Katrak & Agarwal 1981; Kabata-Pendias & Mukherjee 2007; Zhao *et al.* 2010; Mayfield & Lewis 2013). Ti is rather immobile in soil profiles and is usually associated with clay mineral assemblages. Due to their stability and their capacity to be transported by different natural agents (e.g. wind, water) in different grain sizes, both elements have been regarded as proxies for dust or sediment input related to soil erosion caused by deforestation and/or other land-use changes (Hölzer & Hölzer 1998; Kempter & Frenzel 1999; Fábregas Valcarce *et al.* 2003; Martínez Cortizas *et al.* 2005). In the case of Håkonshella, the lack of correlation between Ga and Al, K, Mn or Fe ($r < 0.16$, $p > 0.29$) indicated that fluctuations of Ga along layer 3 were most likely not driven by edaphological factors or mineral inputs from the surrounding slopes. The latter also applied to Ti, which showed a different pattern to those of Al and Si ($r < 0.25$, $p > 0.17$). Whereas Al and Si were highly correlated ($r = 0.84$, $p < 0.0001$) and precisely reflected the variations in the input of coarse material along C1, as confirmed by thin sections and FA, Ti contents in the coarsest deposit (layer 2) were as low as in layer 1, which showed the finest texture. This suggests that Ti entered the stratigraphy through a different depositional agent from that of Al or Si. We hypothesize that higher Ga and Ti contents in layer 3 mainly entered C1 as dust particles during periods of higher anthropic activity and transformation of the surrounding landscape, probably leading to forest clearances and destabilization of the soil. Although at a lower resolution (five samples, one every 3 cm), pollen analyses from the same stratigraphical sequence indicated significant fluctuations in pollen grains from *Alnus*, *Coryla* and *Betula* (from 30 to 10%) along layer 3 (Overland 2013), probably reflecting changes in forest composition caused by humans in the Mesolithic period.

Si/Al or Si/Ti ratios – the former contributing negatively to F2 –have been widely used as a proxy for biogenic silica, e.g. phytoliths and diatoms (Brown *et al.* 2007; Brown 2011; Stolze *et al.* 2012). Phytoliths, microscopic silica bodies produced by plants, have been consistently found in archaeological settings, often indicating *in situ* processing of plants (Piperno 1988, 2006). Diatoms, unicellular algae organisms occurring in freshwater and marine environments, have previously been found in various archaeological contexts, including in buildings where they indicate the use of turf (Bathurst *et al.* 2010), in agrarian terraces (Trombold & Israde-Alcantara 2005), embedded in the clay used to craft pottery (Matiskainen & Alhonen 1984; Battarbee 1988) and in the filling of canals (Purdue & Berger 2015). The Si/Al values and F2 scores recorded here are strongly negatively correlated ($r = -0.78$, $p < 0.0001$), the four highest peaks in the Si/Al ratio matching the four lowest scores for F2 (Fig. 6). Although somewhat counterintuitive, this points towards more deposition of biogenic silica during periods of site abandonment rather than during site frequentation. This might be explained by the rewetting of the ground and subsequent plant colonization following the periodical abandonments of the settlement, a context that might have favoured a higher deposition of diatoms and phytoliths. The alternation between drier and wetter conditions as cycles related to intervals of occupation and abandonment also explain the comparatively higher presence of redoximorphic features in thin section in layer 3, which indicate changes in the oxidation state of the groundmass (Lindbo *et al.* 2010).

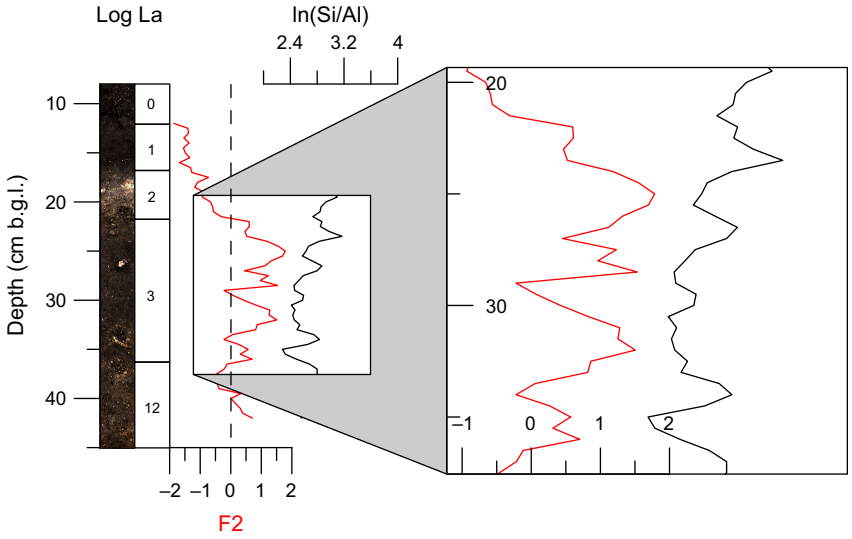

Fig. 6. Comparison between F2 and the Si/Al ratio. Note the correspondence between the highest scores for F2 and the lowest values for the Si/Al ratio ($r = -0.79$, $p < 0.0001$). This figure is available in colour at http://www.boreas.dk.

More information is needed in order to clarify whether climatic shifts were the main factor determining the frequentation/abandonment phases of the Håkonshella hunter-fisher-gatherer settlement. The data available to date do not allow to rule out alternating wet and dry conditions being the result of settlement phases rather than changing climatic conditions, with fires, hearths and site caring temporarily drying out the ground during periods of occupation. In either case, the first hunter-fisher-gatherers in Håkonshella settled directly on the beach surface, as suggested by the coarse nature of microfacies 12a, which shows abundant quartz sand grains and phosphate nodules.

Conclusions

The integration of XRF core scanning with bulk analysis, soil micromorphology and multivariate statistics allows phases of occupation in Scandinavian open-air coastal archaeological settlements to be distinguished, even in homogeneous deposits lacking biogenic carbonate remains and discriminant macrobotanical remains. Authigenic enrichments and depletions of mobile elements can also be identified, providing critical information on diagenesis, anthropic inputs and site formation processes. At Håkonshella we identified four intervals of site occupation and abandonment during the ~1000 years of Mesolithic settlement (6647–6463 to 5620–5486 BC (2σ)). Periods of occupation were characterized by peaks in P, Ga, Ti and higher redoximorphic features. Stages of abandonment were associated with higher Si/Al ratios and organic matter inputs, probably reflecting the periodical return of the natural vegetation and the re-wetting of the site. The definitive abandonment of the settlement was followed by fast burial by colluvium, indicating slope erosion possibly due to changing climatic conditions or loss of vegetation cover. Later, the depression in which the site lies was filled with water for significant periods of time, allowing the formation of a seasonal pond surrounded by hygrophilous plants (probably *Alnus* sp.). These two depositional events contributed to the isolation of the Mesolithic layer from external disturbances, allowing the chemical signals related to the settlement sequences to be preserved through time.

The refinement of our understanding of settlement sequences in massive organic rich deposits has great potential to improve the interpretation of cultural layers in open-air coastal Scandinavian archaeological sites. In the case of Norwegian Mesolithic societies, this will lead to enhanced insights into mobile settlement patterns and site-occupation frequencies, thus contributing to our knowledge on the degree of sedentariness of specialized Mesolithic maritime societies. From a methodological standpoint, the application of XRF core scanning in archaeological settings will probably enhance sampling precision, as microstratigraphical layers containing traces of human activity are likely to be identified. Being a relatively fast, non-destructive technique, the data obtained through XRF core scanning may also be useful for archaeologists to re-arrange digging strategies while still in the field.

Acknowledgements. – Prof. Marco Madella (ICREA–Universitat Pompeu Fabra) and Dr Welmoed Out (Christian–Albrechts–Universität zu Kiel) helped to identify the pollen anthers. Dr Jaime Frigola (Universitat de Barcelona) provided critical help during XRF core scanning. Many thanks also to the reviewers and the Editor of Boreas (Prof. Jan A. Piotrowski) for their valuable comments on an earlier version of the manuscript. All mistakes and shortcomings remain our own.

References

Åstveit, L. I. 2009: Different ways of building, different ways of living: Mesolithic house structures in western Norway. *In* McCartan, S., Schulting, R., Warren, G. & Woodman, P. (eds.): *Mesolithic Horizons*, 414–421. Oxbow Books, Oxford.

Attaelmanan, A. G. & Mouton, M. 2014: Identification of archaeological potsherds excavated at Mleiha using XRF. *Journal of Archaeological Science 42*, 519–524.

Bahr, A., Jimenez-Espejo, F. J., Kolasinac, N., Grunert, P., Hernández-Molina, F. J., Röhl, U., Voelker, A. H. L., Escutia, C., Stow, D. A. V., Hodell, D. & Alvarez-Zarikian, C. A. 2014: Deciphering bottom current velocity and paleoclimate signals from contourite deposits in the Gulf of Cádiz during the last 140 kyr: an inorganic geochemical approach. *Geochemistry, Geophysics, Geosystems 18*, 3145–3160.

Bailey, G. & Flemming, N. 2008: Archaeology of the continental shelf: marine resources, submerged landscapes and underwater archaeology. *Quaternary Science Reviews 27*, 2153–2165.

Balbo, A. L., Madella, M., Vila, A. & Estévez, J. 2010a: Micromorphological perspectives on the stratigraphical excavation of shell middens: a first approximation from the ethnohistorical site Tunel VII, Tierra del Fuego (Argentina). *Journal of Archaeological Science 37*, 1252–1259.

Balbo, A. L., Persson, P. & Roberts, S. J. 2010b: Changes in settlement patterns on the River Rena, southeast Norway: a response to Holocene climate change? *The Holocene 20*, 917–929.

Bathurst, R. R., Zori, D. & Byock, J. 2010: Diatoms as bioindicators of site use: locating turf structures from the Viking Age. *Journal of Archaeological Science 37*, 2920–2928.

Battarbee, R. W. 1988: The use of diatom analysis in archaeology: a review. *Journal of Archaeological Science 15*, 621–644.

Bergsvik, K. A. 2002: Arkeologiske undersøkelser ved Skatestraumen. *Arkeologiske avhandlinger og rapporter fra Universitetet i Bergen 7*, 169 pp.

Bethell, P. & Máté, I. 1989: The use of soil phosphate analysis in archaeology: a critique. *In* Henderson, J. (ed.): *Scientific Analysis in Archaeology*, 1–29. Oxford University Committee for Archaeology, Oxford.

Bjerck, H. B. 2005: Colonizing seascapes: comparative perspectives on the development of maritime relations in the Pleistocene/Holocene transition in north-west Europe. *In* McCartan, S., Schulting, R., Warren, G. & Woodman, P. (eds.): *Mesolithic Horizons. Papers Presented at the Seventh International Conference on the Mesolithic in Europe, Belfast 2005*, 16–23. Oxbow Books, Oxford.

Bjerck, H. B. 2008: Norwegian Mesolithic trends: a review. *In* Bailey, G. & Spikins, P. (eds.): *Mesolithic Europe*, 60–106. Cambridge University Press, Cambridge.

Bjerck, H. B., Åstveit, L. I., Meling, T., Gundersen, J., Jørgensen, G. & Normann, S. 2008: *NTNU Vitenskapsmuseets Arkeologiske Undersøkelser. Ormen Lange Nyhamna*. 70 pp. Tapir Academic Press, Trondheim.

Bondevik, S. & Svendsen, J. 1998: Distinction between the Storegga tsunami and the Holocene marine transgression in coastal basin deposits of western Norway. *Journal of Quaternary 13*, 529–537.

Briz Godino, I., Álvarez, M., Balbo, A. L., Zurro, D., Madella, M., Villagrán, X. & French, C. 2011: Towards high-resolution shell midden archaeology: experimental and ethnoarchaeology in Tierra del Fuego (Argentina). *Quaternary International 239*, 125–134.

Bronk Ramsey, C. 2009: Bayesian analysis of radiocarbon dates. *Radiocarbon 51*, 337–360.

Brown, E. T. 2011: Lake Malawi's response to 'megadrought' terminations: sedimentary records of flooding, weathering and erosion. *Palaeogeography, Palaeoclimatolology, Palaeoecolology 303*, 120–125.

Brown, E. T., Johnson, T., Scholz, C., Cohen, A. & King, J. 2007: Abrupt change in tropical African climate linked to the bipolar seesaw over the past 55 000 years. *Geophysical Research Letters 34*, L20702, doi: 10.1029/2007GL031240.

Calò, C., Henne, P. D., Eugster, P., van Leeuwen, J., Gilli, A., Hamann, Y., La Mantia, T., Pasta, S., Vescovi, E. & Tinner, W. 2013: 1200 years of decadal-scale variability of Mediterranean vegetation and climate at Pantelleria Island, Italy. *The Holocene 23*, 1477–1486.

Chen, J., Chen, Y., Liu, L., Ji, J., Balsam, W., Sun, Y. & Lu, H. 2006: Zr/Rb ratio in the Chinese loess sequences and its implication for changes in the East Asian winter monsoon strength. *Geochimicha et Cosmochimica Acta 70*, 1471–1482.

Clift, P. D., Wan, S. & Blusztajn, J. 2014: Reconstructing chemical weathering, physical erosion and monsoon intensity since 25 Ma in the northern South China Sea: a review of competing proxies. *Earth-Science Reviews 130*, 86–102.

Columbu, S., Antonelli, F., Lezzerini, M., Miriello, D., Adembri, B. & Blanco, A. 2014: Provenance of marbles used in the Heliocaminus Baths of Hadrian's Villa (Tivoli, Italy). *Journal of Archaeological Science 49*, 332–342.

Courty, M. A., Goldberg, P. & Macphail, R. I. 1989: *Soils and Micromorphology in Archaeology*. 344 pp. Cambridge University Press, Cambridge.

Cronbach, L. J. 1951: Coefficient alpha and the internal structure of tests. *Psychometrika 22*, 297–334.

Cuven, S., Francus, P. & Lamoureux, S. 2011: Mid to Late Holocene hydroclimatic and geochemical records from the varved sediments of East Lake, Cape Bounty, Canadian High Arctic. *Quaternary Science Reviews 30*, 2651–2665.

Davison, W. 1993: Iron and manganese in lakes. *Earth-Science Reviews 34*, 119–163.

Duran, A., Perez-Rodriguez, J. L., Jimenez de Haro, M. C., Franquelo, M. L. & Robador, M. D. 2011: Analytical study of Roman and Arabic wall paintings in the Patio De Banderas of Reales Alcazares' Palace using non-destructive XRD/XRF and complementary techniques. *Journal of Archaeological Science 38*, 2366–2377.

Dypvik, H. & Harris, N. 2001: Geochemical facies analysis of fine-grained siliciclastics using Th/U, Zr/Rb and (Zr/Rb)/Sr ratios. *Chemical Geology 181*, 131–146.

Estévez, J., Villagrán, X., Balbo, A. L. & Hardy, K. 2013: Microtaphonomy in archaeological sites: the use of soil micromorphology to better understand bone taphonomy in archaeological contexts. *Quaternary International 330*, 3–9.

Fábregas Valcarce, R., Martínez Cortizas, A., Blanco Chao, R. & Chesworth, W. 2003: Environmental change and social dynamics in the second–third millennium BC in NW Iberia. *Journal of Archaeological Science 30*, 859–871.

FAO 2006: *World Reference Base for Soil Resources. A Framework for International Classification, Correlation and Communication*. 128 pp. Publishing Management Service, Rome.

Ferro-Vázquez, C., Martínez-Cortizas, A., Nóvoa-Muñoz, J. C. & Ballesteros-Arias, P. 2014: 1500 years of soil use reconstructed from the chemical properties of a terraced soil sequence. *Quaternary International 346*, 28–40.

Finlayson, C., Pacheco, F. G., Rodríguez-Vidal, J., Fa, D. A., Gutierrez López, J. M., Santiago Pérez, A., Finlayson, G., Allue, E., Baena Preysler, J., Cáceres, I., Carrión, J. S., Fernández Jalvo, Y., Gleed-Owen, C. P., Jimenez Espejo, F. J., López, P., López Sáez, J. A., Riquelme Cantal, J. A., Sánchez Marco, A., Guzman, F. G., Brown, K., Fuentes, N., Valarino, C. A., Villalpando, A., Stringer, C. B., Martinez Ruiz, F. & Sakamoto, T. 2006: Late survival of Neanderthals at the southernmost extreme of Europe. *Nature 443*, 850–853.

Forouzan, F., Glover, J. B., Williams, F. & Deocampo, D. 2012: Portable XRF analysis of zoomorphic figurines, 'tokens', and sling bullets from Chogha Gavaneh, Iran. *Journal of Archaeological Science 39*, 3534–3541.

Fossen, H. 1989: Geology of the Minor Bergen Arc, West Norway. *Norges Geologiske Undersøkelse 416*, 47–62.

Frigola, J., Moreno, A., Cacho, I., Canals, M., Sierro, F. J., Flores, J. A., Grimalt, J. O., Hodell, D. A. & Curtis, J. H. 2007: Holocene climate variability in the western Mediterranean region from a deep-water sediment record. *Paleoceanography 22*, PA2209, doi: 10.1029/2006PA001307.

Gardiner, D. T. & James, S. 2012: Wet soil redox chemistry as affected by organic matter and nitrate. *American Journal of Climate Change 1*, 205–209.

Graham, M. C., Gavin, K. G., Farmer, J. G., Kirika, A. & Britton, A. 2002: Processes controlling the retention and release of manganese in the organic-rich catchment of Loch Bradan, SW Scotland. *Applied Geochemistry 17*, 1061–1067.

Grützner, J. & Higgins, S. M. 2010: Threshold behavior of millennial scale variability in deep water hydrography inferred from a 1.1 Ma long record of sediment provenance at the southern Gardar Drift. *Paleoceanography 25*, PA4204, doi: 10/29/2009PA001873.

Haenssler, E., Unkel, I., Dörfler, W. & Nadeau, M. 2014: Driving mechanisms of Holocene lagoon development and barrier accretion in Northern Elis, Peloponnese, inferred from the sedimentary record of the Kotychi Lagoon. *Quaternary Science Journal 63*, 60–77.

Heiri, O., Lotter, A. & Lemcke, G. 2001: Loss on ignition as a method for estimating organic and carbonate content in sediments: reproducibility and comparability of results. *Journal of Paleolimnology 25*, 101–110.

Hodson, M. E. 2002: Experimental evidence for mobility of Zr and other trace elements in soils. *Geochimica et Cosmochimica Acta 66*, 819–828.

Holliday, V. T. & Gartner, W. 2007: Methods of soil P analysis in archaeology. *Journal of Archaeological Science 34*, 301–333.

Hölzer, A. & Hölzer, A. 1998: Silicon and titanium in peat profiles as indicators of human impact. *The Holocene 8*, 685–696.

Hu, D., Clift, P. D., Böning, P., Hannigan, R., Hillier, S., Blusztajn, J., Wan, S. & Fuller, D. Q. 2013: Holocene evolution in weathering and erosion patterns in the Pearl River delta. *Geochemistry, Geophysics, Geosystems 14*, 2349–2368.

Hunt, A. M. W. & Speakman, R. J. 2015: Portable XRF analysis of archaeological sediments and ceramics. *Journal of Archaeological Science 53*, 626–638.

Iriarte, E., Simões, C. D., Diniz, M. & Arias, P. 2013: *High resolution XRF chemostratigraphy of the Poças de São Bento shell midden*. Poster presented at Muge Congress, 150th anniversary of the discovery of the Mesolithic shell middens, March 2013, Salvaterra de Magos, Portugal. Available at: https://www.researchgate.net/publication/259439672_High_resolution_XRF_chemostratigraphy_of_the_Poas_de_So_Bento_shell_midden_%28Sado_estuary_Portugal%29; accessed 7th December 2015.

Jolliffe, I. T. 2002: *Principal Component Analysis*. 405 pp. Springer, London.

Kabata-Pendias, A. & Mukherjee, A. B. 2007: *Trace Elements from Soil to Human*. 550 pp. Springer, Berlin.

Kaiser, H. F. 1960: The application of electronic computers to factor analysis. *Educational and Psychology Measurement 20*, 141–151.

Kaiser, H. F. 1974: An index of factorial simplicity. *Psychometrika 39*, 32–36.

Kaiser, H. F. & Rice, J. 1974: Little Jiffy, Mark IV. *Educational and Psychology Measurement 34*, 111–117.

Kalbe, J., Mischke, S., Dulski, P. & Sharon, G. 2014: The Middle Palaeolithic Nahal Mahanayeem Outlet site, Israel: reconstructing the environment of Late Pleistocene wetlands in the eastern Mediterranean from ostracods. *Journal of Archaeological Science 54*, 385–395.

Karkanas, P. & Goldberg, P. 2010: Phosphatic features. *In* Stoops, G., Marcelino, V. & Mees, F. (eds.): *Interpretation of Micromorphological Features of Soils and Regoliths*, 521–541. Elsevier, Oxford.

Katrak, F. E. & Agarwal, J. C. 1981: Gallium: long-run supply. *Journal of Metals 33*, 33–36.

Kempter, H. & Frenzel, B. 1999: The local nature of anthropogenic emission sources on the elemental content of nearby ombrotrophic peat bogs, Vulkaneifel, Germany. *Science of the Total Environment 241*, 117–128.

Koinig, K., Shotyk, W., Lotter, A. & Ohlendorf, C. 2003: 9000 years of geochemical evolution of lithogenic major and trace elements in the sediment of an alpine lake–the role of climate, vegetation, and land-use history. *Journal of Paleolimnology 4*, 307–320.

Kylander, M. E., Ampel, L., Wohlfarth, B. & Veres, D. 2011: High-resolution X-ray fluorescence core scanning analysis of Les Echets (France) sedimentary sequence: new insights from chemical proxies. *Journal of Quaternary Science 26*, 109–117.

Lindbo, D. L., Stolt, M. H. & Vepraskas, M. J. 2010: Redoximorphic features. *In* Stoops, G., Marcelino, V. & Mees, F. (eds.): *Interpretation of Micromorphological Features of Soils and Regoliths*, 129–147. Elsevier, Oxford.

Liu, L., Chen, J., Ji, J., Chen, Y. & Balsam, W. 2006: Variation of Zr/Rb ratios in the Chinese loess deposits during the past 1.8 Myr and its implication for the change of East Asian monsoon intensity. *Geochemistry, Geophysics, Geosystems 7*, 1–9.

Liu, S., Li, Q. H., Gan, F., Zhang, P. & Lankton, J. W. 2012: Silk Road glass in Xinjiang, China: chemical compositional analysis and interpretation using a high-resolution portable XRF spectrometer. *Journal of Archaeological Science 39*, 2128–2142.

Löwemark, L., Chen, H. F., Yang, T. N., Kylander, M., Yu, E. F., Hsu, Y. W., Lee, T. Q., Song, S. R. & Jarvis, S. 2011: Normalizing XRF-scanner data: a cautionary note on the interpretation of high-resolution records from organic-rich lakes. *Journal of Asian Earth Sciences 40*, 1250–1256.

Martin, L., Mooney, S. & Goff, J. 2014: Coastal wetlands reveal a non-synchronous island response to sea-level change and a palaeostorm record from 5.5 kyr to present. *The Holocene 24*, 569–580.

Martínez Cortizas, A., Mighall, T., Pontevedra Pombal, X., Novoa Munfoz, J. C., Peiteado Varela, E. & Piñeiro Rebolo, R. 2005: Linking changes in atmospheric dust deposition, vegetation change and human activities in northwest Spain during the last 5300 years. *The Holocene 15*, 698–706.

Matiskainen, H. & Alhonen, P. 1984: Diatoms as indicators of provenance in Finnish sub-Neolithic pottery. *Journal of Archaeological Science 11*, 147–157.

Mayfield, D. B. & Lewis, A. S. 2013: *Environmental review of coal ash as a resource for rare earth and strategic elements*. 2013 World of Coal Ash (WOCA) Conference in Lexington, KY. Available at: http://www.flyash.info/2013/051-Mayfield-2013.pdf (accessed 19th November 2015).

McGowan, G. & Prangnell, J. 2007: The significance of vivianite in archaeological settings. *Geoarchaeology 21*, 93–111.

Miot, J., Benzerara, K., Morin, G., Bernard, S., Beyssac, O., Larquet, E., Kappler, A. & Guyot, F. 2009: Transformation of vivianite by anaerobic nitrate-reducing iron-oxidizing bacteria. *Geobiology 7*, 373–384.

Morellón, M., Valero-Garcés, B., Vegas-Vilarrúbia, T., González-Sampériz, P., Romero, Ó., Delgado-Huertas, A., Mata, P., Moreno, A., Rico, M. & Corella, J. P. 2009: Late glacial and Holocene palaeohydrology in the western Mediterranean region: The Lake Estanya record (NE Spain). *Quaternary Science Reviews 28*, 2582–2599.

Moreno, A., Pérez, A., Frigola, J., Nieto-Moreno, V., Rodrigo-Gámiz, M., Martrat, B., González-Sampériz, P., Morellón, M., Martín-Puertas, C., Corella, J. P., Belmonte, Á., Sancho, C., Cacho, I., Herrera, G., Canals, M., Grimalt, J. O., Jiménez-Espejo, F., Martínez-Ruiz, F., Vegas-Vilarrúbia, T. & Valero-Garcés, B. L. 2012: The Medieval Climate Anomaly in the Iberian Peninsula reconstructed from marine and lake records. *Quaternary Science Reviews 43*, 16–32.

Mücher, H., van Steijn, H. & Kwaad, F. 2010: Colluvial and mass wasting deposits. *In* Stoops, G., Marcelino, V. & Mees, F. (eds.): *Interpretation of Micromorphological Features of Soils and Regoliths*, 37–48. Elsevier, Oxford.

Olsen, A. B. 1992: *Kotedalen – en Boplass Gjennom 5000 år. Bd. 1. Fangstbosetning og Tidlig Jordbruk i Vestnorsk Steinalder*. 150 pp. Universitetet i Bergen, Bergen.

Overland, A. 2013: *Paleobotaniske analyser ved Håkonshella, Bergen Kommune, Hordaland*. 30 pp. Universitetet i Bergen, Bergen.

Piga, G., Santos-Cubedo, A., Moya Solà, S., Brunetti, A., Malgosa, A. & Enzo, S. 2009: An X-ray diffraction (XRD) and X-ray fluorescence (XRF) investigation in human and animal fossil bones from Holocene to Middle Triassic. *Journal of Archaeological Science 36*, 1857–1868.

Piperno, D. 1988: *Phytolith Analysis: An Archaeological and Geological Perspective*. 280 pp. Academic Press, San Diego.

Piperno, D. 2006: *Phytoliths. A Comprehensive Guide for Archaeologists and Paleoecologists*. 238 pp. Altamira Press, Oxford.

Poto, L., Gabrieli, J., Crowhurst, S. J., Appleby, P. G., Ferretti, P., Surian, N., Cozzi, G., Zaccone, C., Turetta, C., Pini, R., Kehrwald, N. & Barbante, C. 2013: The first continuous Late Glacial – Holocene peat bog multi-proxy record from the Dolomites (NE Italian Alps). *Quaternary International 306*, 71–79.

Purdue, L. E. & Berger, J. 2015: An integrated socio-environmental approach to the study of ancient water systems: the case of prehistoric Hohokam irrigation systems in semi-arid central Arizona, USA. *Journal of Archaeological Science 53*, 586–603.

Ramstad, M. 2005: Island settlements and maritime hunter-fishers: spatial and temporal transformations over 11 000 years at Melkøya, northern Norway. *In* McCartan, S., Schulting, R., Warren, G. & Woodman, P. (eds.): *Mesolithic Horizons*, 422–429. Oxbow Books, Oxford.

Reimer, P. J., Bard, E., Bayliss, A., Beck, J. W., Blackwell, P. G., Bronk, C., Caitlin, R., Hai, E. B., Edwards, R. L., Friedrich, M., Grootes, P. M., Guilderson, T. P., Haflidason, H., Hajdas, I., Hatté, C., Heaton, T., Hoffmann, D. L., Hogg, A. G., Hughen, K. A., Kaiser, K. F., Kromer, B., Manning, S. W., Niu, M., Reimer, R. W., Richards, D. A., Marian Scott, E., Southon, J. R., Staff, R. A., Turney, C. S. M. & van der Plicht, J. 2013: IntCal13 and Marine13 radiocarbon age calibration curves 0–50 000 years cal bp. *Radiocarbon 55*, 1869–1887.

Schittek, K., Forbriger, M., Mächtle, B., Schäbitz, F., Wennrich, V., Reindel, M. & Eitel, B. 2014: Holocene environmental changes in the highlands of the southern Peruvian Andes (14°S) and their impact on pre-Columbian cultures. *Climate of the Past 10*, 1707–1746.

Shilstein, S. S. & Shalev, S. 2011: Making sense out of cents: compositional variations in European coins as a control model for archaeometallurgy. *Journal of Archaeological Science 38*, 1690–1698.

Simpson, D. N. 1999: Lithic raw material frequencies and the construction of site chronology: the Neolithic phases of Kotedalen, Western Norway. *In* Boaz, J. (ed.): *The Mesolithic of Central Scandinavia*, 299–316. Universitets Oldsaksamling, Oslo.

Stolze, S., Dörfler, W., Monecke, T. & Nelle, O. 2012: Evidence for climatic variability and its impact on human development during the Neolithic from Loughmeenaghan, County Sligo, Ireland. *Journal of Quaternary Science 27*, 393–403.

Stoops, G. 2003: *Guidelines for Analysis and Description of Soil and Regolith Thin Sections*. 184 pp. Soil Society of America, Inc., Madison.

Stoops, G., Marcelino, V. & Mees, F. (eds.) 2010: *Interpretation of Micromorphological Features of Soils and Regoliths*. 752 pp. Elsevier, Amsterdam.

Thurstone, L. L. 1947: *Multiple Factor Analysis*. 535 pp. University of Chicago Press, Chicago.

Trombold, C. & Israde-Alcantara, I. 2005: Paleoenvironment and plant cultivation on terraces at La Quemada, Zacatecas, Mexico: the pollen, phytolith and diatom evidence. *Journal of Archaeological Science 32*, 341–353.

Unkel, I., Björck, S. & Wohlfarth, B. 2008: Deglacial environmental changes on Isla de los Estados (54.4°S), southeastern Tierra del Fuego. *Quaternary Science Reviews 27*, 1541–1554.

Villagrán, X., Balbo, A. L., Madella, M., Vila, A. & Estévez, J. 2011: Stratigraphic and spatial variability in shell middens: microfacies identification at the ethnohistoric site Tunel VII (Tierra del Fuego, Argentina). *Archaeological and Anthropological Sciences 34*, 357–378.

Wedepohl, K. H. 1971: *Geochemistry*. 231 pp. Holt, Reinhart and Winston, New York.

Weltje, G. J. & Tjallingii, R. 2008: Calibration of XRF core scanners for quantitative geochemical logging of sediment cores: theory and application. *Earth and Planetary Science Letters 274*, 423–438.

Zhao, X., Qin, S., Yang, Y., Li, Y. & Lin, M. 2010: Concentration of gallium in the Permo-Carboniferous coals of China. *Energy, Exploration and Exploitation 27*, 333–344.

Supporting Information

Additional Supporting Information may be found in the online version of this article at http://www.boreas.dk.

Table S1. XRF data set.